

Dependence of Land Surface Albedo on Solar Zenith Angle: Observations and Model Parameterization

FANGLIN YANG

Science Applications International Corporation, and NCEP Environmental Modeling Center, Camp Springs, Maryland

KENNETH MITCHELL AND YU-TAI HOU

NCEP Environmental Modeling Center, Camp Springs, Maryland

YONGJIU DAI

State Key Laboratory of Remote Sensing Science, School of Geography, Beijing Normal University, Beijing, China

XUBIN ZENG AND ZHUO WANG

Department of Atmospheric Sciences, The University of Arizona, Tucson, Arizona

XIN-ZHONG LIANG

Illinois State Water Survey, Department of Natural Resources, University of Illinois at Urbana-Champaign, Urbana, Illinois

(Manuscript received 30 July 2007, in final form 18 March 2008)

ABSTRACT

This study examines the dependence of surface albedo on solar zenith angle (SZA) over snow-free land surfaces using the intensive observations of surface shortwave fluxes made by the U.S. Department of Energy Atmospheric Radiation Measurement (ARM) Program and the National Oceanic and Atmospheric Administration Surface Radiation Budget Network (SURFRAD) in 1997–2005. Results are used to evaluate the National Centers for Environmental Prediction (NCEP) Global Forecast Systems (GFS) parameterization and several new parameterizations derived from the Moderate Resolution Imaging Spectroradiometer (MODIS) products. The influence of clouds on surface albedo and the albedo difference between morning and afternoon observations are also investigated. A new approach is taken to partition the observed upward flux so that the direct-beam and diffuse albedos can be separately computed. The study focused first on the ARM Southern Great Plains Central Facility site. It is found that the diffuse albedo prescribed in the NCEP GFS matched closely with the observations. The direct-beam albedo parameterized in the GFS is largely underestimated at all SZAs. The parameterizations derived from the MODIS product underestimated the direct-beam albedo at large SZAs and slightly overestimated it at small SZAs. Similar results are obtained from the analyses of observations at other stations. It is also found that the morning and afternoon dependencies of direct-beam albedo on SZA differ among the stations. Attempts are made to improve numerical model algorithms that parameterize the direct-beam albedo as a product of the direct-beam albedo at $SZA = 60^\circ$ (or the diffuse albedo), which varies with surface type or geographical location and/or season, and a function that depends only on SZA. A method is presented for computing the direct-beam albedos over these snow-free land points without referring to a particular land-cover classification scheme, which often differs from model to model.

1. Introduction

Surface albedo is one of the most important parameters that affect the earth's surface energy budget. It is

a major source of uncertainties in radiative transfer calculations. In this study we use the U.S. Department of Energy Atmospheric Radiation Measurement (ARM) Program (Stokes and Schwartz 1994; Ackerman and Stokes 2003) and the National Oceanic and Atmospheric Administration Surface Radiation Budget Network (SURFRAD) (Augustine et al. 2000) observations to evaluate and improve the parameterizations of

Corresponding author address: Fanglin Yang, NCEP/EMC, 5200 Auth Road, Camp Springs, MD 20746.
E-mail: fanglin.yang@noaa.gov

the solar zenith angle (SZA)–albedo relationship for climate and weather forecast models.

Land surface albedos over both bare soil and plant canopies have a strong dependence on solar zenith angle and the surface characteristics. Since the surface types change considerably from place to place and throughout a growing season, it is a formidable problem to develop different schemes to model the dependence of surface albedo on SZA for different surface types (Briegleb et al. 1986). Dickinson (1983) described a scheme for a semi-infinite canopy consisting of randomly oriented leaves, that is,

$$\alpha(\theta) = \alpha_0 \frac{1 + d}{1 + 2d \cos(\theta)}, \quad (1)$$

where $\theta = \text{SZA}$, $\alpha(\theta)$ is surface albedo at a given θ , α_0 is the albedo at $\cos(60^\circ) = 0.5$, and d is a constant. This scheme was intended for broadband solar flux and made no differentiation between direct-beam and diffuse fluxes.

In its subsequent applications this scheme was modified and expanded to parameterize the albedo–SZA relationship over all snow-free land points (Briegleb et al. 1986; Briegleb 1992; Hou et al. 2002). For example, Briegleb (1992) added the spectral dependence of surface albedo on SZA to the scheme for the then National Center for Atmospheric Research (NCAR) Community Climate Model. They set α_0 differently for the visible (0.2–0.7 μm) and near-infrared (NIR) (0.7–5.0 μm) bands and differently for different land surface types based on various observations, and further prescribed d to be 0.4 for arable land, grassland, and desert (where the dependence of surface albedo on SZA is strong) and d to be 0.1 for all other land surface types (where the dependence of surface albedo on SZA is weak). Briegleb (1992) did not differentiate between direct-beam and diffuse fluxes for the surface downward solar fluxes and used the same relation for both. Since surface albedo for the diffuse flux does not depend on the solar zenith angle, Hou et al. (2002) further modified the scheme described in Briegleb (1992) and applied it only for computing the direct-beam surface albedo as a function of SZA; that is,

$$\alpha_{\text{dir}}^{m,n}(\theta, \lambda) = \alpha_{\text{diff}}^{m,n}(\lambda) \frac{1 + d^n}{1 + 2d^n \cos(\theta)}, \quad (2)$$

where λ designates spectral wavelength band, $\alpha_{\text{diff}}^{m,n}(\lambda)$ is the diffuse albedo [prescribed differently for the ultraviolet and visible band (0.175–0.7 μm) and the near-infrared band (0.7–10 μm), and differently for each vegetation class (index n) in a different month or season (index m)], d^n equals 0.4 (0.1) for vegetation classes

where the albedo has a strong (weak) SZA dependence, and $\alpha_{\text{dir}}^{m,n}(\theta, \lambda)$ is the direct-beam albedo at a given θ . The values of $\alpha_{\text{diff}}^{m,n}(\lambda)$ were obtained from the land use and surface albedo dataset given by Matthews (1983, 1984). This scheme is presently used in the operational National Centers for Environmental Prediction (NCEP) Global Forecast System (GFS) to compute surface radiative fluxes.

It should be pointed out that in modern land surface models (e.g., Bonan 1996; Koster et al. 2000; Dai et al. 2003) separate surface albedos are usually computed for bare soil and vegetation and then combined. The model albedo for bare soil depends on soil moisture and soil color types, and does not depend on SZA. The model albedo for vegetation depends on vegetation characteristics such as leaf and stem area index and vegetation optical property, and on SZA for the solar direct-beam flux. It is either parameterized by a simplified two-stream solution under certain constraints (e.g., Dai et al. 2003) or explicitly resolved by canopy radiative-transfer equations (Bonan 1996; Dai et al. 2004; Oleson et al. 2004). In the schemes described in Briegleb (1992) and Hou et al. (2002), although vegetation albedo is not explicitly represented, it can be regarded as being implicitly resolved by the prescribed surface albedo α_0 or α_{diff} , which does vary with surface soil and vegetation class.

The Dickinson (1983) parameterization and its variations (e.g., Briegleb et al. 1992; Hou et al. 2002) were derived from limited observations. Its accuracy has been an ongoing subject of discussion. In particular, there is a lack of observations with sufficient solar angular resolution for verifying the SZA dependence (Lyapustin 1999). In recent years significant progress has been made in the modeling of land surface albedo since the high-quality fine-resolution satellite measurements from the Moderate Resolution Imaging Spectroradiometer (MODIS; Schaaf et al. 2002) became available. For example, using the MODIS Bidirectional Reflectance Distribution Function (BRDF)/Albedo Model Parameter product, Wang et al. (2007) derived a two-parameter scheme for computing the direct-beam (black sky) albedo and its SZA dependence over land for climate and weather forecast models; that is,

$$\alpha_{\text{dir}}^{m,n}(\theta, \lambda) = \alpha_{\text{dir}}^{m,n}(60^\circ, \lambda) \{1 + B_1^n [g_1(\theta) - g_1(60^\circ)] + B_2^n [g_2(\theta) - g_2(60^\circ)]\}, \quad (3)$$

where $\alpha_{\text{dir}}^{m,n}(60^\circ, \lambda)$ is the direct-beam albedo at 60° and varies with season and vegetation class. The functions $g_1(\theta)$ and $g_2(\theta)$ are derived from a polynomial estimation of the anisotropy model operationally provided as the MODIS model parameter product (see Wang et al.

2007). The two parameters B_1^n and B_2^n vary with vegetation class but are independent of season. Wang et al. (2007) also parameterized the albedo $\alpha_{\text{dir}}^{m,n}(\theta, \lambda)$ following the Dickinson (1983) approach, that is,

$$\alpha_{\text{dir}}^{m,n}(\theta, \lambda) = \alpha_{\text{dir}}^{m,n}(60^\circ, \lambda) \frac{1 + c^n}{1 + 2c^n \cos(\theta)}. \quad (4)$$

Here the parameter c^n is defined differently than the parameter d^n in (2), and is obtained by minimizing the difference between the MODIS operationally retrieved albedo values and the albedo computed from (4) over all SZAs for each vegetation class. Wang et al. (2007) found that c^n changes considerably among vegetation classes and is very different from the two constants given in Briegleb et al. (1986).

The schemes described so far (1)–(4) parameterize surface albedo as a function of SZA and vegetation class. They do not treat bare-soil albedo and vegetation albedo separately as most modern land surface models do (e.g., Bonan 1996; Koster et al. 2000; Dai et al. 2003). Starting with the NCAR Common Land Model (CLM) surface albedo algorithm, Liang et al. (2005) developed a new dynamical–statistical albedo scheme for snow-free land surfaces using the MODIS operational albedo and vegetation products along with soil moisture products from a land data assimilation system. The albedo over vegetation was separate from that over bare soil. Unlike the NCAR CLM in which the bare-soil albedo is a function of soil moisture and soil color type and does not vary with SZA, Liang et al. (2005) parameterized the bare-soil albedo as a product of two terms where one is a function of soil moisture and the other a function of SZA. The bare-soil direct-beam albedo [(7) of Liang et al. 2005] can be rewritten as

$$\alpha_{\text{dir}}^{m,n}(\theta, \lambda) = \alpha_{\text{dir}}^n(\lambda)|_{\mu=0, \psi=0} [1 + C_{1,\lambda} \cos(\theta) + C_{2,\lambda} \cos^2(\theta)] F(\psi, \lambda), \quad (5)$$

where $\mu = \cos(\theta)$, $F(\psi, \lambda)$ is a function of wavelength and soil moisture (ψ) that changes with season m , $C_{1,\lambda}$ ($C_{2,\lambda}$) equals -0.718 (0.346) for the visible band and -0.732 (0.362) for the near-infrared band, and $\alpha_{\text{dir}}^n(\lambda)|_{\mu=0, \psi=0}$ refers to the maximum background soil albedo that varies with land cover type and is defined differently for the visible and near-infrared bands. Liang et al. (2005) demonstrated that this new scheme remarkably improved the accuracy of the surface albedo calculation compared to the one in the NCAR CLM. The dependence of bare-soil albedo on SZA is important and cannot be ignored as most current land surface models do. In this study, the parameterization of vegetation albedo by Liang et al. (2005) is not

included in the validation against ground observations because in this parameterization the SZA dependence cannot be separated from other factors such as leaf and stem areas indices that affect the vegetation albedo [see (9) of Liang et al. 2005].

Remarkable progress has been made using the MODIS products to understand the surface albedo characteristics and to improve the parameterization of surface albedo in numerical models (e.g., Lucht et al. 2000; Wang et al. 2004; Liang et al. 2005; Wang et al. 2007). Still, the dependence of surface albedo on SZA derived from the MODIS data requires further evaluation. First, the MODIS data are not reliable near dusk or dawn for $\text{SZA} > 70^\circ$ [i.e. $\cos(\theta) < 0.34$] when the atmospheric aerosol correction of the input data degrades and the BRDF models themselves grow weak (Liang et al. 2005). Second, the MODIS products are derived under clear-sky conditions and are not suitable for examining the variation of surface albedo with clouds.

Therefore, long-term measurements of surface solar fluxes with high accuracy and fine solar angular resolution are required for a better understanding of the albedo–SZA relationship. The ARM and SURFRAD surface observation networks provide excellent means for us to revisit the albedo–SZA relationships described in Briegleb (1992) and Hou et al. (2002) and those recently derived from the MODIS products (e.g., Liang et al. 2005; Wang et al. 2007). The ARM Program was established in the early 1990s and has been making intensive and continuous measurements of surface solar radiative fluxes and atmospheric quantities at the ARM surface sites in the U.S. Southern Great Plains (SGP), the Northern Slope of Alaska, and in the tropical western Pacific (TWP) islands of Manus and Nauru. The SURFRAD network was established in 1993 and began to collect data in 1995, and is currently operating in seven climatologically diverse regions in Montana, Colorado, Illinois, Mississippi, Pennsylvania, Nevada, and South Dakota. These measurements have been used in the past to improve our understanding of the cloud–radiation interaction and to evaluate model simulations and satellite retrievals of surface radiative fluxes and albedo (e.g., Long and Ackerman 1997; Minnis et al. 1997; Morcrette 2002; Jin et al. 2003; Roesch et al. 2004).

The paper is organized in the following way: we will first focus on the ARM observations at the SGP Central Facility (CF) site to establish the methodology and then apply it to other stations to study the dependencies of surface albedo on SZA over different land surface types. The observations and data processing strategies are described in section 2. Section 3 presents the diffuse albedos derived from the observations at the SGP CF

TABLE 1. Station name, location, surface type, amount of qualified 3-min mean samples, and the percentage (%) of subgroup samples used for computing different albedos at the three ARM and six SURFRAD stations. Values in the parentheses are for clear-sky cases at the ARM SGP CF site.

Station	Location	Surface type	Years of data	No. of samples	α_{diff} (%)	α_{dir} (%)	α_{dir} (%) at SZA = 60°
ARM SGP CF	(36.61°N, 97.49°W)	Pastures	1997–2004	405 915	19.1	74.4 (43.1)	3.6 (2.0)
ARM TWP Manus	(2.01°S, 147.42°E)	Grasses	2001–04	257 142	8.5	65.0	1.6
ARM TWP Nauru	(0.52°S, 166.92°E)	Bare soil	2001–04	184 536	5.2	81.1	1.9
Bondville, IL	(40.05°N, 88.37°W)	Prairie grasses with a few trees	1997–2005	390 663	2.8	88.3	3.6
Table Mountain, CO	(40.13°N, 105.24°W)	Rocky desert with scrub vegetation	1997–2005	514 108	2.7	89.4	3.6
Fort Peck, MT	(48.31°N, 105.10°W)	Prairie grasses with a few trees	1997–2005	410 843	2.9	89.1	3.3
Goodwin Creek, MS	(34.25°N, 89.87°W)	Pasture grasses with a few deciduous trees	1997–2005	495 219	2.3	90.1	3.5
Penn State, PA	(40.72°N, 77.93°W)	Grasses and crops	1998–2005	325 631	3.5	86.3	3.3
Sioux Falls, SD	(43.73°N, 96.62°W)	Prairie grasses	2003–05	132 031	2.4	90.4	3.4

and compares them with those prescribed in the NCEP GFS. Section 4 presents the direct-beam albedos at the SGP CF. The difference in albedo between morning and afternoon observations is examined. The diffuse and direct-beam albedos obtained in sections 3 and 4 are then used in section 5 to evaluate the NCEP GFS and MODIS-based parameterizations described above. In section 6, the analysis is extended to the other ARM stations and SURFRAD stations over different land surface types. Two generalized functions that describe the dependencies of normalized direct-beam albedo on SZA are derived from the observations made at eight ARM and SURFRAD stations. Section 7 gives a summary of this study.

2. ARM and SURFRAD observations

The observational data used for this study were obtained from the ARM Climate Research Facility Data Archive (<http://www.arm.gov/data/>) and the SURFRAD Network Web site (<http://www.srrb.noaa.gov/surfrad/>). Both the ARM and SURFRAD instruments measure surface downward total and diffuse fluxes and the surface upward total flux. We used the Value-Added Best-Estimate Radiative Flux (BEFLUX) product (Shi and Long 2002) at the SGP CF, the Ground and Sky Radiation Sensors measured fluxes at the TWP Manus and Nauru Islands, and the Active Remotely-Sensed Clouds Locations (ARSCL) product (Clothiaux et al. 2001) at all three ARM sites. Details about instruments, data processing, and quality controls can be found in the aforementioned references and on the two Web sites. Based on the availability of both radiation and cloud products, this study uses the ARM observations

at the SGP CF site for 1997–2004 and at the TWP Manus and Nauru Islands for 2001–04. A solar positioning algorithm (available online at <http://www.squ1.com/>) was used to compute solar zenith angles at 1-min temporal resolution in accordance with the time and location of the observations. Even though most of the SURFRAD stations began to collect data in 1995, 1997 was the first year that measurements of diffuse fluxes were available throughout the entire year. Table 1 lists the names and locations of the ARM and SURFRAD stations, together with the years and amounts of data used at each station.

The SURFRAD surface radiative fluxes are provided as 3-min means. The radiation and cloud data we acquired from the ARM archive are in 1-min and 10-s temporal resolutions. For this study all ARM data as well as the SZA were resampled as 3-min means. The 10-s ARSCL cloud-base distributions in each 3-min period were used to derive cloud occurrence frequency (cloud cover). We also tested 5- and 10-min samplings and obtained almost identical results. However, 1-h sampling degrades the solar angular resolution. We opted to use the 3-min sampling to take advantage of the high solar angular resolution.

As an example, in Fig. 1a we show the diurnal variation of surface total albedo at the SGP CF site in 2003. Here total albedo is defined as the ratio between the surface upward and the surface downward total short-wave (SW) fluxes. The radiation instruments at the SGP CF site are situated on a pasture field. The albedo varied with the time of the day and the season, and was usually larger at dawn and dusk than at noon. It was in the range of 0.1 to ~0.3 except for days when the ground was covered by snow (see the yellow and red

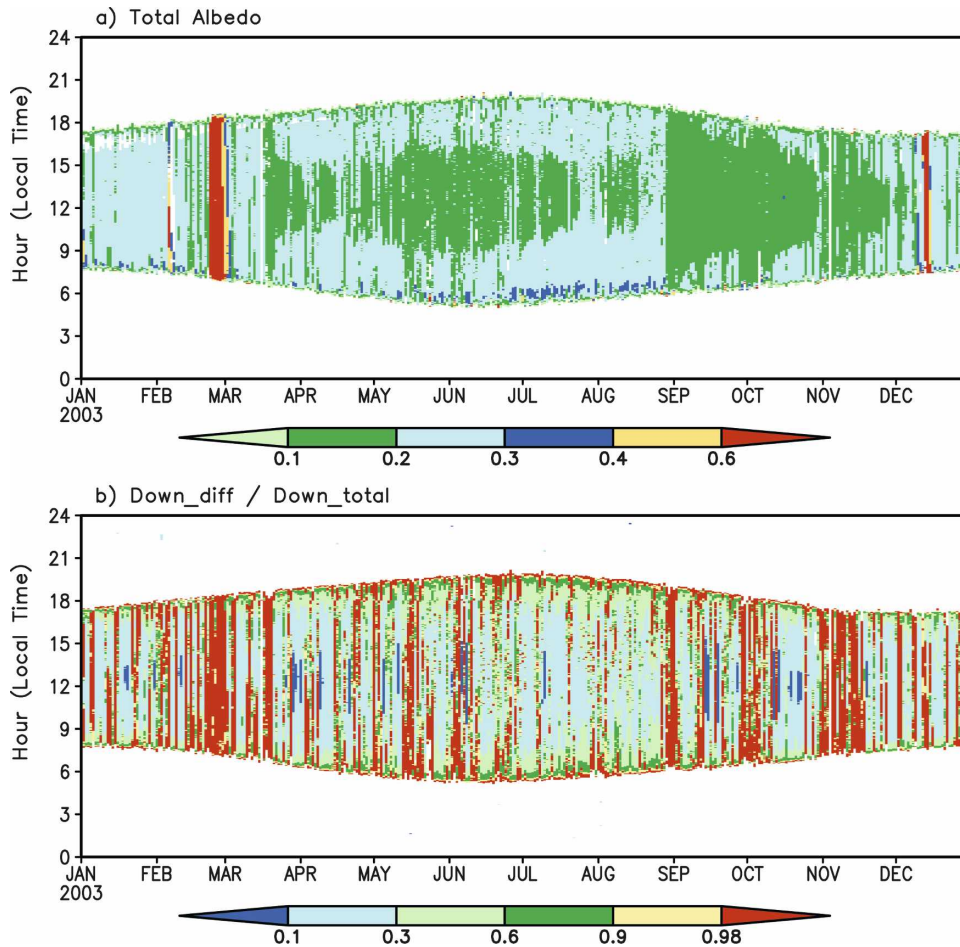


FIG. 1. Diurnal and seasonal variations of (a) surface albedo and (b) the ratio between the downward diffuse and the downward total solar fluxes at the ARM SGP CF in 2003. In (a), the albedo is for the total flux, which includes both the direct-beam and diffuse solar fluxes.

shadings in Fig. 1a). For this study, data samples at all stations with surface total albedo greater than 0.35 were excluded from the analysis. We further excluded those samples that had a downward or upward flux smaller than 5 W m^{-2} , which is within the instrument uncertainties (<http://www.arm.gov>). The number of qualified samples at each station is given in Table 1, together with the percentage of subset samples used for different applications.

It should be pointed out that one difficulty in evaluating model parameterizations using point observations lies in the incompatibility in space and time between point observations and model grid values. Point observations do not always represent well model grid values, especially when the comparison is made for a specific time slice. Usually, large samples of observations have to be collected. Then, model grid values are compared to the means and their higher moments of the samples over a certain period based on the premise that the

limitation in spatial coverage of the observations is offset by the temporal averaging. For example, Barnett et al. (1998) investigated the temporal and spatial scales of surface shortwave fluxes measured at the ARM SGP sites and the Oklahoma MESONET. They showed that the temporal correlation between the fluxes measured at the SGP CF and the mean over an area $60 \text{ km} \times 60 \text{ km}$ is about 0.7 for cloudy-sky conditions and 0.8 for clear-sky conditions. Long et al. (2002) examined total cloud amount over the SGP network measured during the ARM 1997 and 2000 cloud intensive operational periods. They found that, in general, the representativeness of the SGP CF cloud cover decreases as the distance used for computing average cloud cover increases. On a daily basis, the average distance is 75–100 km for a correlation of 0.8–0.9. Yang et al. (2006) further examined how the temporal mean of point observations in a given period is related to area mean if the advection of air masses is considered. These studies

suggest that if handled properly, certain pointwise observations can be useful for evaluating model grid values. In this study, long-term observations at high-temporal resolutions and at a variety of ground observation stations are used for making comparisons with model grid values. We shall focus on the bulk features of the observations and their long-term mean statistics.

3. Diffuse albedo at the SGP CF site

It is known that the albedos for direct-beam and diffuse fluxes have different characteristics. The diffuse albedo does not change with SZA while the direct-beam albedo does. Therefore, it is necessary to treat them differently. The ARM instruments measure surface downward total and diffuse fluxes and the surface upward total flux. To separately derive the direct-beam and diffuse albedos from the ARM data, one has to partition the measured upward flux into two parts, one associated with the downward direct-beam flux and the other with the downward diffuse flux. A new method is introduced below for this partitioning.

Because of scattering by atmospheric constituents, a portion of the downward solar flux is composed of the diffuse flux. Usually the ratio of downward diffuse flux to downward total flux increases as SZA increases. It also increases as cloud amount increases. As an example, we show in Fig. 1b the ratio between the downward diffuse flux and the downward total flux at the SGP CF site in 2003. At many points the ratios were larger than 0.98, which occurred exclusively under overcast conditions (red color in Fig. 1b). These points are scattered through the year and occurred at different times of the day. In other words, their occurrences were not biased toward any particular season or time of the day. Based on this observation, we picked a subset of the 3-min mean samples for which the aforementioned ratios were larger than 0.98. The samples satisfying this condition accounted for 19.1% of the 405 915 total samples at the SGP CF site in 1997–2004 (see Table 1). Two more tests were carried out with the critical ratio being set to 0.99 and 0.999. No significant changes were found in the derived diffuse albedos described below. The critical ratio of 0.98 was finally chosen for maximizing the sample size for all stations and for making the results robust. We then calculated the diffuse albedo as the ratio between the total upward and total downward fluxes from this subset. Figure 2 shows, as an example, the distributions of the diffuse albedo as a function of the cosine of SZA in January, April, July, and October, respectively. The most prominent feature is that the diffuse albedo does not strongly vary with SZA for $\cos(\text{SZA})$ in the range of 0.2–1.0. However, it

tends to either slightly increase or decrease with SZA for $\cos(\text{SZA})$ smaller than 0.2. This might be caused by the multiple scattering of diffuse fluxes that depend on SZA as explained by Pinty et al. (2005). On the other hand, this may result from our data processing. For certain samples, the downward diffuse fluxes still contain up to 2% of direct-beam fluxes, which do depend on SZA, especially at sunrise and sunset times.

The above albedos obtained from individual samples were then used to compute monthly-mean diffuse albedo for each of the months in the 8 yr and the 8-yr means of monthly-mean diffuse albedos (Fig. 3). It should be pointed out that these diffuse albedos are based on spectrally integrated fluxes. In numerical models the diffuse albedos are usually defined differently for the ultraviolet and visible band (UVV) than for the near-infrared band since surface albedo changes sharply from the visible to near-infrared spectrum for the majority of land surface types. In the NCEP GFS, the diffuse albedo $\alpha_{\text{diff}}^{mn}(\lambda)$ in (2) is prescribed differently for different months and differently for the UVV and NIR bands. We computed the spectrally integrated diffuse albedo by linearly combining the two GFS broadband albedos together with two weighting coefficients, which are the fractions of solar energy in each band relative to the solar constant as defined at the top of the atmosphere. The coefficients are 0.47047 for the UVV band and 0.52953 for the NIR band.

Thus, Fig. 3 compares the spectrally integrated monthly-mean diffuse albedos we derived from ARM SGP observations with those prescribed in the GFS. The numbers for all stations are given in Table 2. The ARM monthly-mean diffuse albedo has large year-to-year variations, probably due to changes in the surface properties. Nevertheless, the GFS monthly-mean albedo is in good agreement with the 8-yr mean ARM albedo for the SGP CF site. Both of them are larger in the northern summer months than in the northern winter months. The GFS diffuse albedos are slightly larger than the observed for the September–November season.

4. Direct-beam albedo at the SGP CF site

After obtaining the spectrally integrated monthly-mean diffuse albedo ($\alpha_{\text{diff}}^{mn}$) for each month in the 8 yr, we calculated the part of the upward solar flux ($F_{\text{dir}}^{\uparrow}$) that was associated with the downward direct-beam flux as

$$F_{\text{dir}}^{\uparrow} = F_{\text{total}}^{\uparrow} - \alpha_{\text{diff}}(F_{\text{total}}^{\downarrow} - F_{\text{dir}}^{\downarrow}), \quad (6)$$

where $F_{\text{total}}^{\downarrow}$, $F_{\text{dir}}^{\downarrow}$, and $F_{\text{total}}^{\uparrow}$ are the downward total SW flux, downward direct-beam SW flux, and upward total SW flux, respectively. These fluxes are available from

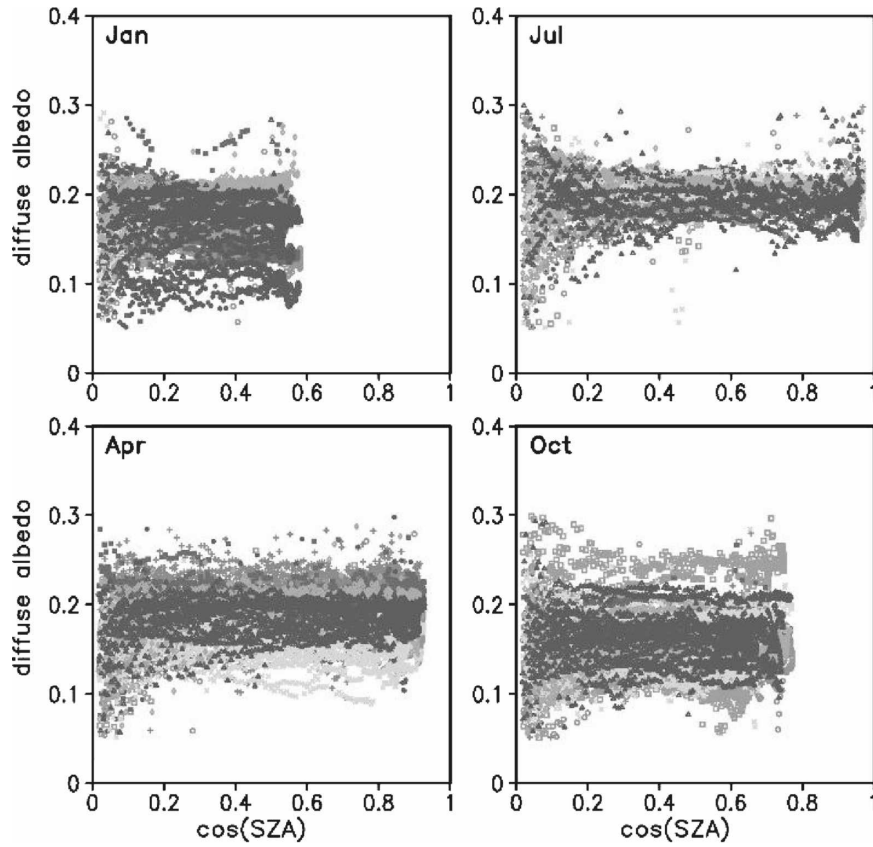


FIG. 2. Distributions of surface diffuse albedo as a function of the cosine of solar zenith angle in January, April, July, and October 1997–2004 at the ARM SGP CF site. Different marks represent data for different years.

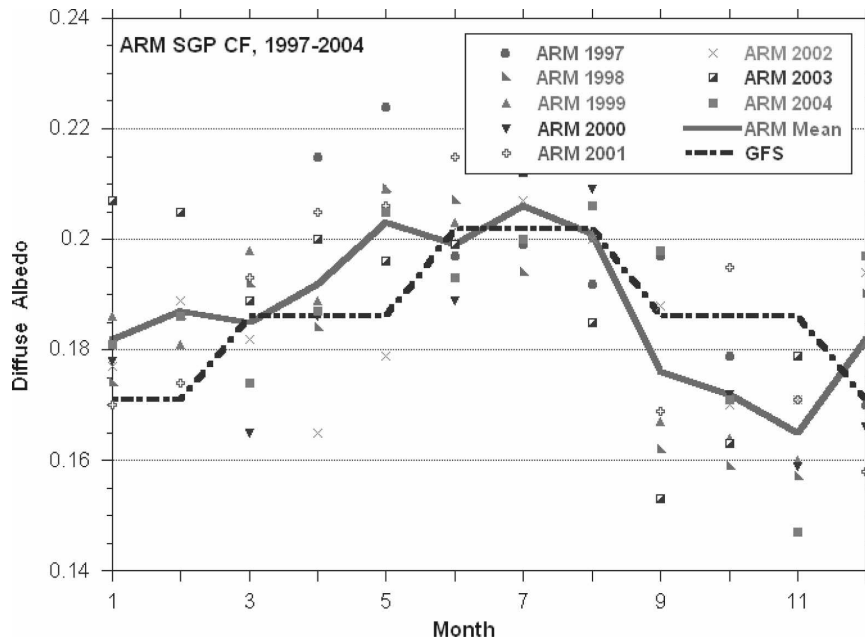


FIG. 3. Monthly-mean diffuse albedos at the SGP CF site derived from the ARM observations and the corresponding diffuse albedos prescribed in NCEP GFS.

TABLE 2. Multiyear mean monthly-mean diffuse albedos derived from the ARM and SURFRAD observations. The diffuse albedos prescribed in the NCEP GFS for the SGP CF site are also included for reference.

	Jan	Feb	Mar	Apr	May	Jun	Jul	Aug	Sep	Oct	Nov	Dec
NCEP GFS for SGP CF	0.171	0.171	0.186	0.186	0.186	0.202	0.202	0.202	0.186	0.186	0.186	0.171
ARM SGP CF	0.182	0.187	0.185	0.192	0.203	0.199	0.206	0.201	0.176	0.172	0.165	0.182
ARM TWP Manus	0.182	0.186	0.192	0.185	0.188	0.190	0.184	0.190	0.186	0.183	0.176	0.182
ARM TWP Nauru	0.188	0.178	0.182	0.194	0.194	0.183	0.183	0.194	0.183	0.182	0.179	0.186
Bondville, IL	0.252	0.249	0.246	0.224	0.218	0.215	0.212	0.214	0.216	0.220	0.228	0.255
Table Mountain, CO	0.176	0.170	0.168	0.162	0.165	0.161	0.163	0.155	0.155	0.152	0.155	0.166
Fort Peck, MT	0.220	0.212	0.182	0.174	0.177	0.166	0.173	0.178	0.185	0.184	0.179	0.195
Goodwin Creek, MS	0.191	0.190	0.194	0.202	0.199	0.196	0.194	0.186	0.178	0.182	0.183	0.196
Penn State, PA	0.233	0.232	0.220	0.200	0.200	0.198	0.204	0.204	0.202	0.198	0.207	0.227
Sioux Falls, SD	0.208	0.231	0.181	0.185	0.183	0.19	0.205	0.197	0.175	0.185	0.191	0.211

the ARM measurements. Considering its large year-to-year variation, the $\alpha_{\text{diff}}^{m,n}$ in each year was used for the calculation instead of the 8-yr mean $\alpha_{\text{diff}}^{m,n}$. Even though $\alpha_{\text{diff}}^{m,n}$ was derived from a subset of the observations taken under overcast conditions, the calculation was applied to all samples under both clear- and cloudy-sky conditions based on the assumption that $\alpha_{\text{diff}}^{m,n}$ does not

change with the sky condition and only depends on the land surface type. Lyapustin (1999) showed that surface albedo is primarily an intrinsic property of the surface characteristics and its dependence on atmospheric conditions is minor.

We show in Fig. 4 the direct-beam albedos $\alpha_{\text{diff}}^{m,n}(\theta)$ at the SGP CF site in 1997–2004 as a function of SZA for

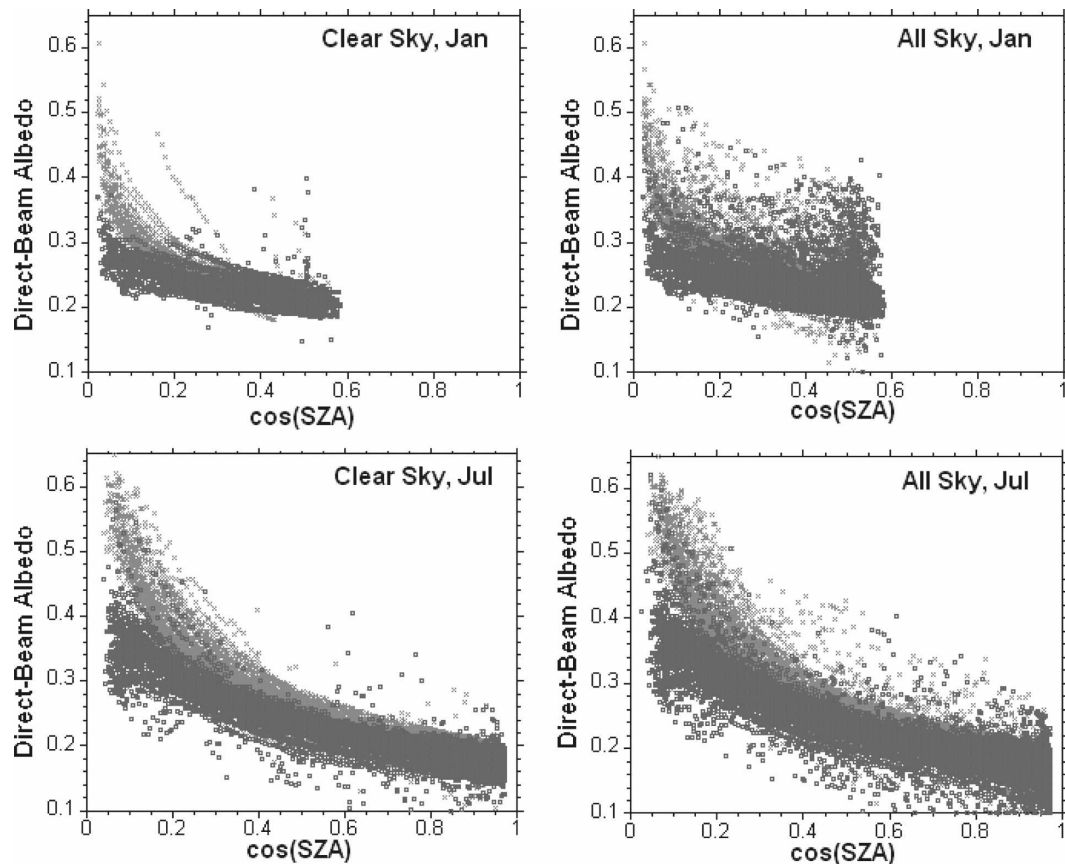


FIG. 4. Scatterplots of direct-beam albedos in (top) January and (bottom) July derived from ARM observations at the SGP CF site for (left) clear-sky and (right) all-sky conditions in 1997–2004. The crosses (squares) represent albedos derived from observations in the morning (afternoon).

January and July under clear- and all-sky conditions. Different symbols are also used to distinguish between the albedos in the morning and afternoon. Unlike the diffuse albedo shown in Fig. 2, the direct-beam albedo strongly depends on SZA. In July the albedo at sunrise and sunset was 2–3 times that at local noon. The difference between clear- and all-sky albedos was small. At a given solar zenith angle the direct-beam albedo in the morning was usually much larger than that in the afternoon, especially at dawn and dusk. We also compared the diffuse albedos between morning and afternoon and found no systematic differences between them (figures not shown). Minnis et al. (1997) examined the diurnal cycle of surface broadband total albedo at a few ARM SGP sites and found that at a given solar zenith angle the total albedo in the morning can be sometimes 10% larger than that in the afternoon at certain stations. They concluded that the asymmetry is primarily caused by the effects of dew on albedo. In section 6 we will show that the asymmetry in the diurnal variation of direct-beam albedo does not always exist at all stations.

5. Normalized direct-beam albedo at the SGP CF site and its parameterizations in the NCEP GFS and derived from the MODIS product

Since the diffuse albedo does not depend on SZA we will no longer consider the parameterization (1), which assumed the same SZA dependence for both the direct and diffuse components. The remaining investigation is focused on how to parameterize the direct-beam albedo as a function of SZA. The diffuse and direct-beam albedos we obtained at the ARM SGP CF site in previous sections are for spectrally integrated solar fluxes. The direct-beam albedos parameterized in (2)–(5) are spectrum dependent. Can we use ARM measurements to evaluate these parameterizations? We introduce here normalized albedos and rewrite the GFS parameterization (2) and the parameterizations (3) and (4) that Wang et al. (2007) derived from MODIS as

$$\frac{\alpha_{\text{dir}}^{m,n}(\theta, \lambda)}{\alpha_{\text{diff}}^{m,n}(\lambda)} = \frac{1 + d^n}{1 + 2d^n \cos(\theta)}, \tag{7}$$

$$\frac{\alpha_{\text{dir}}^{m,n}(\theta, \lambda)}{\alpha_{\text{dir}}^{m,n}(60^\circ, \lambda)} = 1 + B_1^n [g_1(\theta) - g_1(60^\circ)] + B_2^n [g_2(\theta) - g_2(60^\circ)], \text{ and } \tag{8}$$

$$\frac{\alpha_{\text{dir}}^{m,n}(\theta, \lambda)}{\alpha_{\text{dir}}^{m,n}(60^\circ, \lambda)} = \frac{1 + c^n}{1 + 2c^n \cos(\theta)}. \tag{9}$$

For a given vegetation class prescribed by the superscript n , the parameters d^n , B_1^n , B_2^n , and c^n are pre-

scribed constants and they do not change with the solar spectrum. The normalized albedos are functions of SZA only. Once these functions are determined and the spectrum-dependent diffuse albedo $\alpha_{\text{diff}}^{m,n}(\lambda)$ for use in (7) or spectrum-dependent direct-beam albedo $\alpha_{\text{dir}}^{m,n}(60^\circ, \lambda)$ for use in (8)–(9) are given, the direct-beam albedos for different solar spectral bands can be obtained. The SGP CF site is covered by pasture. The corresponding values of the parameters given in the NCEP GFS and Wang et al. (2007) are $d^n = 0.4$, $B_1^n = 0.57$, $B_2^n = 0.12$, and $c^n = 0.26$. The functions $g_1(\theta)$ and $g_2(\theta)$ are described in Wang et al. (2007).

Since the functions on the right-hand sides of (7)–(9) do not depend on the solar spectrum, it is easy to prove that

$$\frac{\alpha_{\text{dir}}^{m,n}(\theta, \lambda)}{\alpha_{\text{diff}}^{m,n}(\lambda)} = \frac{\alpha_{\text{dir}}^{m,n}(\theta)}{\alpha_{\text{diff}}^{m,n}} \text{ and } \tag{10}$$

$$\frac{\alpha_{\text{dir}}^{m,n}(\theta, \lambda)}{\alpha_{\text{diff}}^{m,n}(60^\circ, \lambda)} = \frac{\alpha_{\text{dir}}^{m,n}(\theta)}{\alpha_{\text{diff}}^{m,n}(60^\circ)}, \tag{11}$$

where the albedos on the left-hand sides are for solar fluxes in each broad band and the albedos on the right-hand sides are for spectrally integrated solar fluxes. This equality allows us to use the ARM measured spectrally integrated solar fluxes to assess the accuracy of the parameterized albedo–SZA relations for individual spectra bands.

The Liang et al. (2005) parameterization (5) was structured differently from the ones above. The albedos over vegetation and bare soil are parameterized differently. The direct-beam albedo over bare soil depends not only on SZA but also on soil moisture. Furthermore, the coefficients C_1 and C_2 in (5) are prescribed differently for the visible and near-infrared bands. Nevertheless, it will be shown that the normalized direct-beam albedo is still only a function of SZA. First, we use (5) to deduce the direct-beam albedos over bare soil at $\text{SZA} = 60^\circ$ for the visible and near-infrared bands and denote them as $\alpha_{\text{dir}}^{\text{vis},m,n}(\theta = 60^\circ) = 0.7275\alpha_{\text{dir}}^{\text{vis},n}|_{\mu=0,\psi=0}F(\psi)$ and $\alpha_{\text{dir}}^{\text{nir},m,n}(\theta = 60^\circ) = 0.7235\alpha_{\text{dir}}^{\text{nir},n}|_{\mu=0,\psi=0}F^{\text{nir}}(\psi)$, respectively. Then, dividing (5) by these two equations we have

$$\frac{\alpha_{\text{dir}}^{\text{vis},m,n}(\theta)}{\alpha_{\text{dir}}^{\text{vis},m,n}(\theta = 60^\circ)} = 1.3745 - 0.9869 \cos(\theta) + 0.4756 \cos^2(\theta) \text{ and } \tag{12}$$

$$\frac{\alpha_{\text{dir}}^{\text{nir},m,n}(\theta)}{\alpha_{\text{dir}}^{\text{nir},m,n}(\theta = 60^\circ)} = 1.3803 - 1.0104 \cos(\theta) + 0.4997 \cos^2(\theta). \tag{13}$$

One can see that the normalized albedos change only with SZA. Although the normalization is performed separately for the visible and near-infrared bands, as Liang et al. (2005) have already pointed out, it turns out that the difference between the two normalized albedos is relatively small (see Fig. 7b). This reinforces the notion that the normalized direct-beam albedo has a weak dependence on the solar spectrum even though the albedo itself usually behaves differently in the visible and near-infrared bands.

a. Fits from the ARM measurements at the SGP CF site

Now that we have converted the parameterizations (2)–(5) for direct-beam albedos into parameterizations (7)–(9), (12), and (13) for normalized direct-beam albedos that depend only on SZA, we now proceed to use the direct-beam and diffuse albedos we derived from the ARM measurements in sections 3 and 4 to assess the accuracy of these parameterizations. The focus is on how the normalized snow-free land surface albedo changes with SZA with or without clouds in the atmosphere.

Figure 5 shows scatterplots of normalized direct-beam albedo $\alpha_{\text{dir}}^{m,n}(\theta)/\alpha_{\text{diff}}^{m,n}$ as a function of $\cos(\theta)$ computed and depicted separately for clear-sky and all-sky conditions using observations in the morning, afternoon, or both (the entire-day cases). Figure 6 is the same as Fig. 5 except for the normalized albedo $\alpha_{\text{dir}}^{m,n}(\theta)/\alpha_{\text{dir}}^{m,n}(60^\circ)$. The computation was carried out month by month in each year using all qualified samples of the direct-beam albedo $\alpha_{\text{dir}}^{m,n}$ and corresponding monthly-mean $\alpha_{\text{diff}}^{m,n}$ and $\alpha_{\text{dir}}^{m,n}(60^\circ)$. The $\alpha_{\text{diff}}^{m,n}$ has been given in section 3 (Fig. 3). We used samples of $\alpha_{\text{dir}}^{m,n}(\theta)$ that satisfy the condition $|\theta - 60^\circ| \leq \Delta\theta$, for small $\Delta\theta$, in each month to compute the monthly mean $\alpha_{\text{dir}}^{m,n}(60^\circ)$ for clear-sky and all-sky conditions and for morning, afternoon, and entire-day cases. For $\Delta\theta = 1^\circ$ averaged for all years and all cases, 2.0% of clear-sky samples and 3.6% of all-sky samples satisfy this condition (Table 1). Table 3 gives the multiyear mean monthly mean $\alpha_{\text{dir}}^{m,n}(60^\circ)$ for the entire-day case at the ARM SGP CF station, together with those at other ARM and SURFRAD stations. We tested the sensitivity of $\alpha_{\text{dir}}^{m,n}(60^\circ)$ by doubling or halving $\Delta\theta$ and found little change in $\alpha_{\text{dir}}^{m,n}(60^\circ)$.

We included in each panel of Figs. 5 and 6 the samples for all years from 1997 through 2004 at the SGP CF site, and tested different fits to obtain an empirical relation that best describes the dependence of normalized direct-beam albedo on SZA. The polynomials shown in Figs. 5 and 6 were ultimately selected for their higher accuracy and for having a format compat-

ible to the current GFS parameterization. The normalized direct-beam albedos in Figs. 5 and 6 all show strong dependencies on SZA. However, the fit for $\alpha_{\text{dir}}^{m,n}(\theta)/\alpha_{\text{diff}}^{m,n}$ differs considerably from that for $\alpha_{\text{dir}}^{m,n}(\theta)/\alpha_{\text{dir}}^{m,n}(60^\circ)$ because the monthly-mean diffuse albedo is consistently smaller than the direct-beam albedo at 60° in all months (see Tables 2 and 3). In the next section we discuss in detail the influence of clouds and the diurnal asymmetry of the albedos and compare the fits with model parameterizations (7), (8), (9), (12), and (13).

b. Model parameterizations versus ARM fits at the SGP CF site

Shown in Fig. 7a are the normalized direct-beam albedo $\alpha_{\text{dir}}^{m,n}(\theta)/\alpha_{\text{diff}}^{m,n}$ as a function of $\cos(\theta)$ from the ARM fits in Fig. 5 and the NCEP GFS parameterization (7) for the SGP CF site. The difference between the fits for clear- and all-sky cases is small. This indicates that the effect of clouds on the direct-beam albedos is negligible. The albedos in the morning are larger than those in the afternoon at large solar zenith angles. Compared to the ARM fits, the GFS parameterization underestimated the direct-beam albedo at all solar zenith angles. The largest bias occurred at sunrise and sunset. Yang et al. (2006) found that the NCEP GFS forecasts overestimated the surface downward SW fluxes at the SGP CF site by up to 50 W m^{-2} at 3 p.m. local time. However, the upward SW fluxes from the forecasts matched rather well with the ARM observations. They pointed out that the discrepancy was likely linked to a low bias in the surface albedo prescribed in the GFS. Our analysis in section 3 showed that the diffuse albedo prescribed in the GFS was relatively accurate. The low bias in GFS surface albedo was primarily caused by the underestimate of direct-beam albedo in the GFS.

Figure 7b compares the normalized direct-beam albedo $\alpha_{\text{dir}}^{m,n}(\theta)/\alpha_{\text{dir}}^{m,n}(60^\circ)$ from the ARM fits in Fig. 6 with those from the parameterizations (8), (9), (12), and (13). The most prominent feature is that the parameterizations Liang et al. (2005) and Wang et al. (2007) derived from the MODIS BRDF product all tend to underestimate the direct-beam albedo at large solar zenith angles and overestimate the direct-beam albedo at small solar zenith angles near local noon. It has been known that MODIS data are not accurate for SZA larger than 70° [$\cos(\theta) < 0.34$]. However, it is not clear why these parameterizations all overestimate the albedo at small solar zenith angles. The constants in these parameterizations were obtained by minimizing the errors between the parameterized albedos and the MODIS mean albedos (Liang et al. 2005; Wang et al. 2007) sampled over a 16-day period. It is possible that this

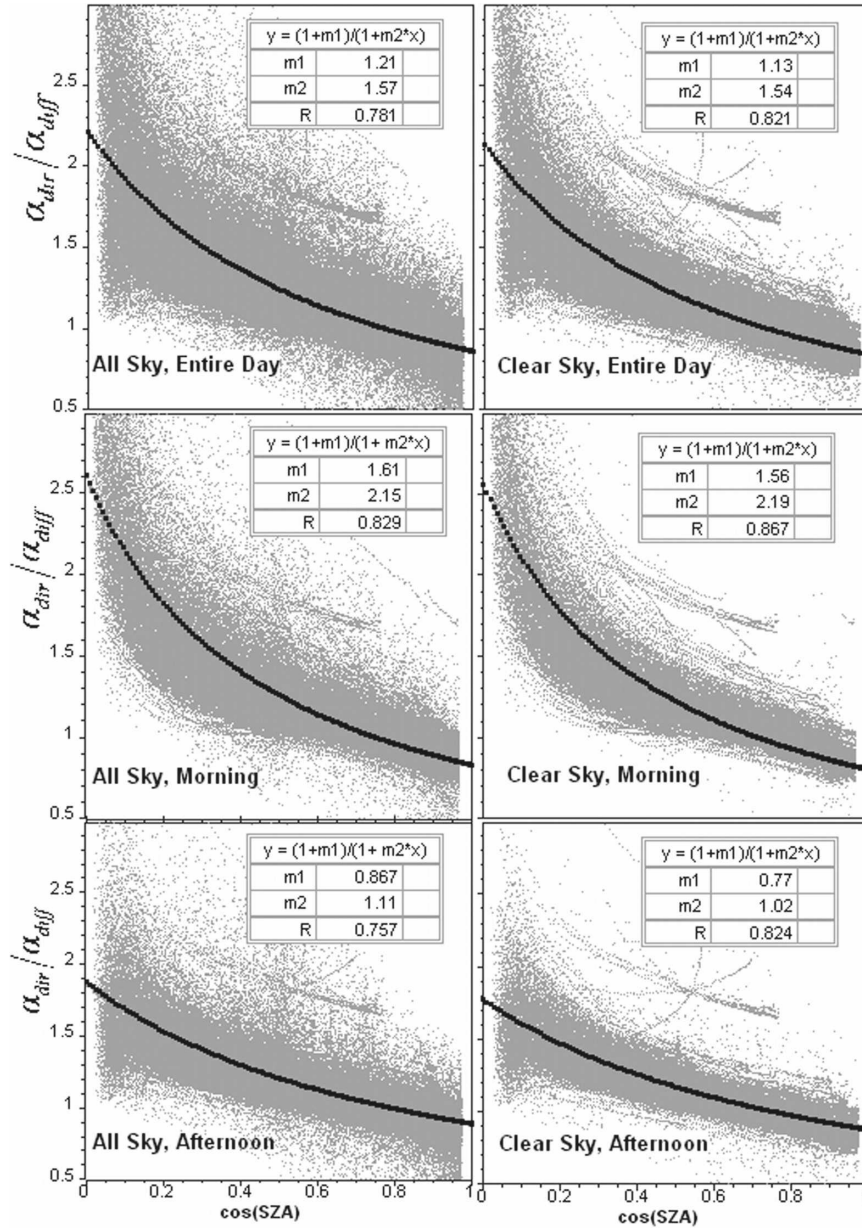


FIG. 5. Distributions of direct-beam albedo normalized by the diffuse albedo vs $\cos(\text{SZA})$ at the SGP CF site in 1997–2004 under (left) clear-sky and (right) all-sky conditions. Included are (middle) the morning, (lower) afternoon, and (upper) entire-day observations. In each panel, the observations are fitted to a polynomial plotted as the thick black line.

procedure led to an overestimate of the direct-beam albedo at small solar zenith angles to compensate for the underestimate of the albedo at large solar zenith angles. It should be pointed out that Jin et al. (2003) performed validations for the MODIS albedo at local noon. They did not find such a uniform overestimate of albedo at small solar zenith angles.

A few more points can be drawn from Fig. 7b. (i) Consistent with the fits for $\alpha_{\text{dir}}^{m,n}(\theta)/\alpha_{\text{diff}}^{m,n}$ in Fig. 7a, the

fits for $\alpha_{\text{dir}}^{m,n}(\theta)/\alpha_{\text{dir}}^{m,n}(60^\circ)$ are almost identical for the clear-sky and all-sky cases. The influence of atmospheric condition on the dependence of the surface albedo on SZA is negligible. (ii) At the SGP CF site, $\alpha_{\text{dir}}^{m,n}(\theta)/\alpha_{\text{dir}}^{m,n}(60^\circ)$ is larger (smaller) in the morning than in the afternoon for solar zenith angles larger (smaller) than 60° . (iii) Even though Wang et al. (2007) and Liang et al. (2005) took totally different approaches to deduce the dependence of direct-beam al-

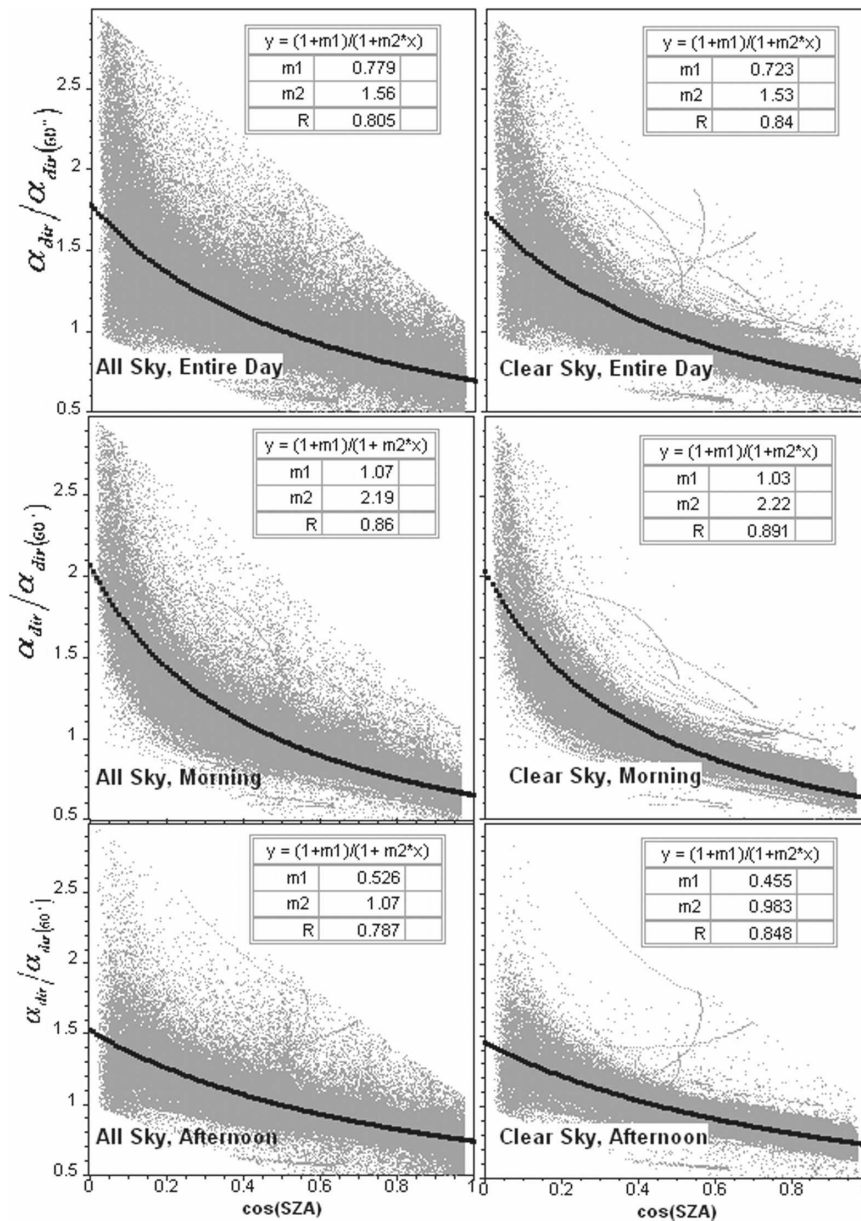


FIG. 6. As in Fig. 5, but the direct-beam albedo is normalized by the direct-beam albedo at 60°.

bedo on SZA using the same MODIS BRDF data, the two-parameter scheme [Eq. (8)] that Wang et al. (2007) obtained is almost identical to either of the schemes that Liang et al. (2005) obtained for different spectral bands. (iv) The normalized direct-beam albedos that Liang et al. (2005) defined separately for the visible and near-infrared bands [(12) and (13)] show almost identical dependencies on $\cos(\theta)$. Therefore, for model parameterizations it is acceptable to use only one function to describe the dependence of the normalized albedo on $\cos(\theta)$ for both spectral bands. The variation in the

nonnormalized direct-beam albedo with wavelength is represented by $\alpha_{dir}^{m,n}(60^\circ, \lambda)$, which is prescribed differently for different spectral bands. (v) The Wang et al. (2007) one-parameter scheme gives the weakest SZA dependence.

As an accuracy assessment, we first computed the surface upward SW flux that is associated with the downward direct-beam flux using either the parameterizations of GFS and Wang et al. (2007) or the ARM fits for entire-day cases in Fig. 7, and the upward SW flux that is associated with the downward diffuse flux using

TABLE 3. Multiyear mean monthly-mean direct-beam albedos at SZA = 60° derived from the ARM and SURFRAD entire-day observations. Missing values (N/A) indicate that the SZA is always >60° in that month.

	Jan	Feb	Mar	Apr	May	Jun	Jul	Aug	Sep	Oct	Nov	Dec
ARM SGP CF	0.232	0.225	0.228	0.231	0.241	0.249	0.241	0.252	0.230	0.229	0.216	0.212
ARM TWP Manus	0.240	0.232	0.226	0.242	0.240	0.232	0.243	0.249	0.240	0.237	0.238	0.246
ARM TWP Nauru	0.268	0.258	0.258	0.267	0.257	0.251	0.244	0.255	0.248	0.238	0.234	0.247
Bondville, IL	0.290	0.278	0.282	0.274	0.277	0.263	0.239	0.239	0.247	0.254	0.258	N/A
Table Mountain, CO	0.186	0.181	0.181	0.187	0.197	0.198	0.198	0.188	0.184	0.174	0.174	N/A
Fort Peck, MT	N/A	0.186	0.194	0.205	0.215	0.211	0.204	0.212	0.212	0.207	N/A	N/A
Goodwin Creek, MS	0.220	0.231	0.233	0.245	0.250	0.244	0.244	0.234	0.224	0.219	0.215	0.215
Penn State, PA	0.249	0.242	0.257	0.245	0.250	0.246	0.252	0.244	0.236	0.226	0.233	N/A
Sioux Falls, SD	N/A	0.204	0.204	0.214	0.230	0.234	0.238	0.228	0.210	0.222	0.218	N/A

the diffuse albedo shown in Fig. 3 and Table 2. The two upward fluxes are then combined and compared to the ARM-measured surface upward total SW flux at the SGP CF site. Presented in Fig. 8 are box plots showing

the median value and quartiles of the differences (biases) between the computed and ARM-measured upward SW fluxes with all of the samples from 1997 to 2004 included. The comparison for the clear-sky case is similar and is not shown. One can see that both the ARM fits and the MODIS-based parameterizations developed by Wang et al. (2007) are capable of accurately reproducing the observed mean upward flux for this time period. Fifty percent of the samples (quartiles) have errors less than about $\pm 5 \text{ W m}^{-2}$ (the first four columns in Fig. 8). The NCEP GFS parameterization systematically underestimated the upward fluxes. The mean bias is about -7 W m^{-2} .

We further divided the samples into five bins with $\cos(\theta)$ being centered at 0.1, 0.3, 0.5, 0.7, and 0.9, respectively. Figure 9 shows the percent errors of the computed surface upward fluxes relative to ARM ob-

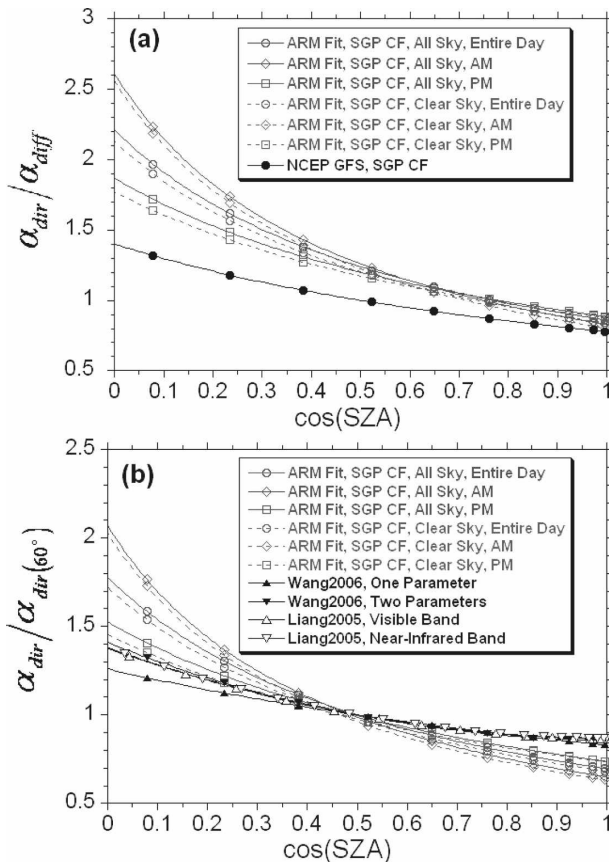


FIG. 7. Dependencies of normalized direct-beam albedo on $\cos(\text{SZA})$ at the ARM SGP CF site as determined by the ARM fits in Figs. 5, 6 and by the parameterizations (7)–(9), (12), and (13). The direct-beam albedo is normalized by (a) the diffuse albedo and (b) the direct-beam albedo at SZA = 60°. The ARM fits were carried out separately for clear- and all-sky conditions, and separately with morning, afternoon, and entire-day observations.

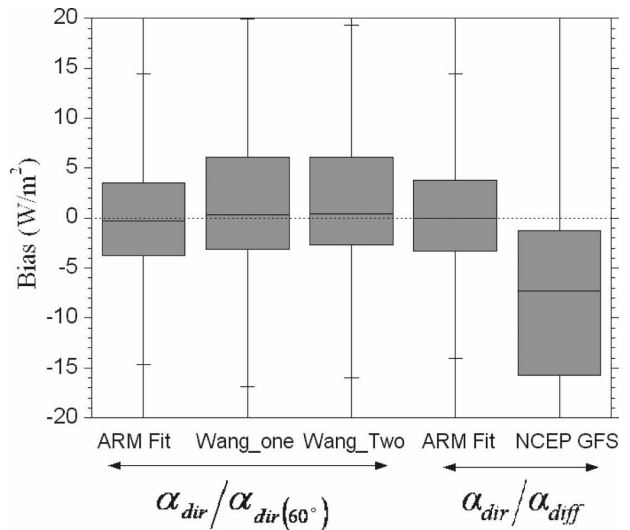


FIG. 8. Box plot showing the median values and quartiles of the biases in the upward (direct and diffuse) SW fluxes (W m^{-2}) between empirical fits and ARM observations at the SGP CF site in 1997–2004. Here the ARM fit refers to the fits in Fig. 7 based on entire-day observations. See text for details.

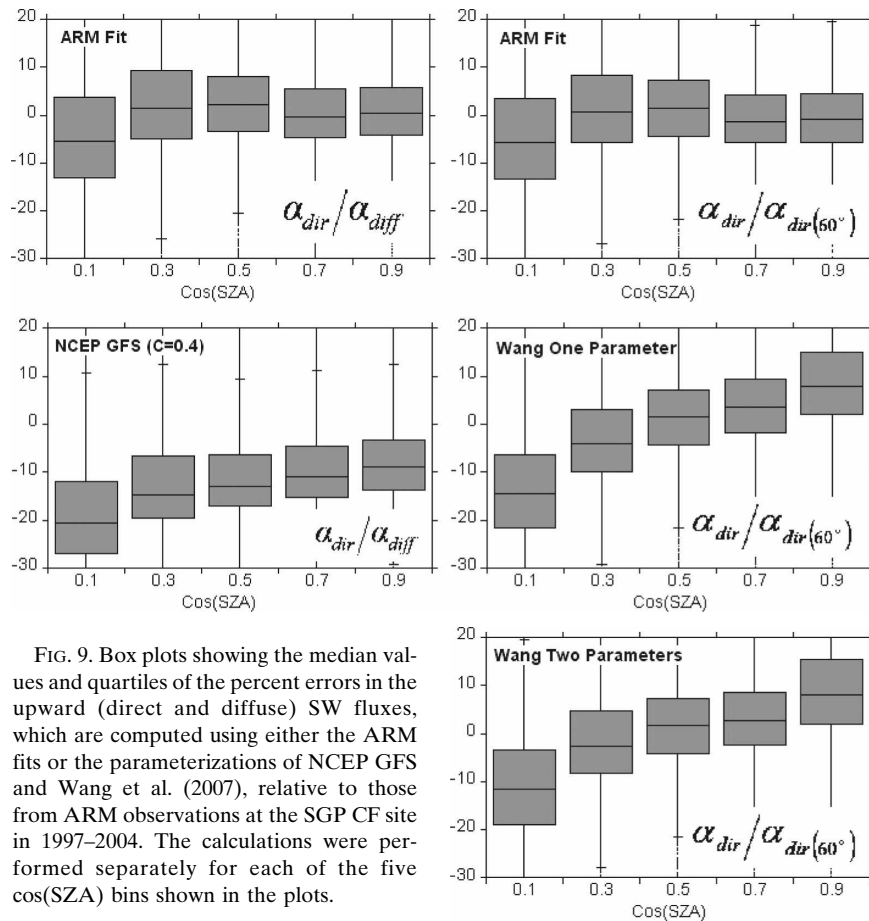


FIG. 9. Box plots showing the median values and quartiles of the percent errors in the upward (direct and diffuse) SW fluxes, which are computed using either the ARM fits or the parameterizations of NCEP GFS and Wang et al. (2007), relative to those from ARM observations at the SGP CF site in 1997–2004. The calculations were performed separately for each of the five cos(SZA) bins shown in the plots.

servations for each of the five bins. The NCEP GFS parameterization underestimated the upward SW fluxes by about 15% at dusk and dawn and by about 10% at local noon. Even though the Wang et al. (2007) parameterizations rather accurately estimated the daily mean fluxes (Fig. 8), they underestimate the fluxes by 6%–9% at dusk and dawn and overestimated them by 9% at local noon. The ARM fits we obtained from this study improved the flux estimation. However, it should be pointed out that the Wang et al. (2007) parameterizations were derived from relatively coarse-resolution footprints of the satellite sensors compared to the ARM pointwise observations. Some of the biases may be introduced by spatial incompatibility.

6. Dependencies of normalized direct-beam albedo on SZA for different surface types

Up to now the analysis has been based only on the observations made at the SGP CF site. In this section we apply the same analysis strategy to the observations

taken at the ARM TWP Manus and Nauru islands and at the six SURFRAD stations to test if and how the albedo–SZA relationships at these stations may differ from those we obtained for the SGP CF site.

The station characteristics and data availabilities are described in Table 1. Following the same procedure described in previous sections we derived for each station first the diffuse and direct-beam albedos and then obtained fits of the normalized direct-beam albedo as a function of SZA under all-sky conditions. The calculations were carried out separately for the morning and afternoon observations and then the entire-day observations. The resultant multiyear monthly-mean diffuse albedo $\alpha_{\text{diff}}^{m,n}$ and direct-beam albedo at 60° $\alpha_{\text{dir}}^{m,n}(60^\circ)$ for the entire-day cases are listed in Tables 2 and 3, respectively. At a few SURFRAD stations, the SZA was always larger than 60° in certain winter months and therefore no monthly-mean $\alpha_{\text{dir}}^{m,n}(60^\circ)$ s were given. One can see that $\alpha_{\text{dir}}^{m,n}(60^\circ)$ is consistently larger than $\alpha_{\text{diff}}^{m,n}$ in all months at all stations. This implies that to have the same direct-beam albedo the constants d in (2) and c in (4) must be prescribed differently for the same surface

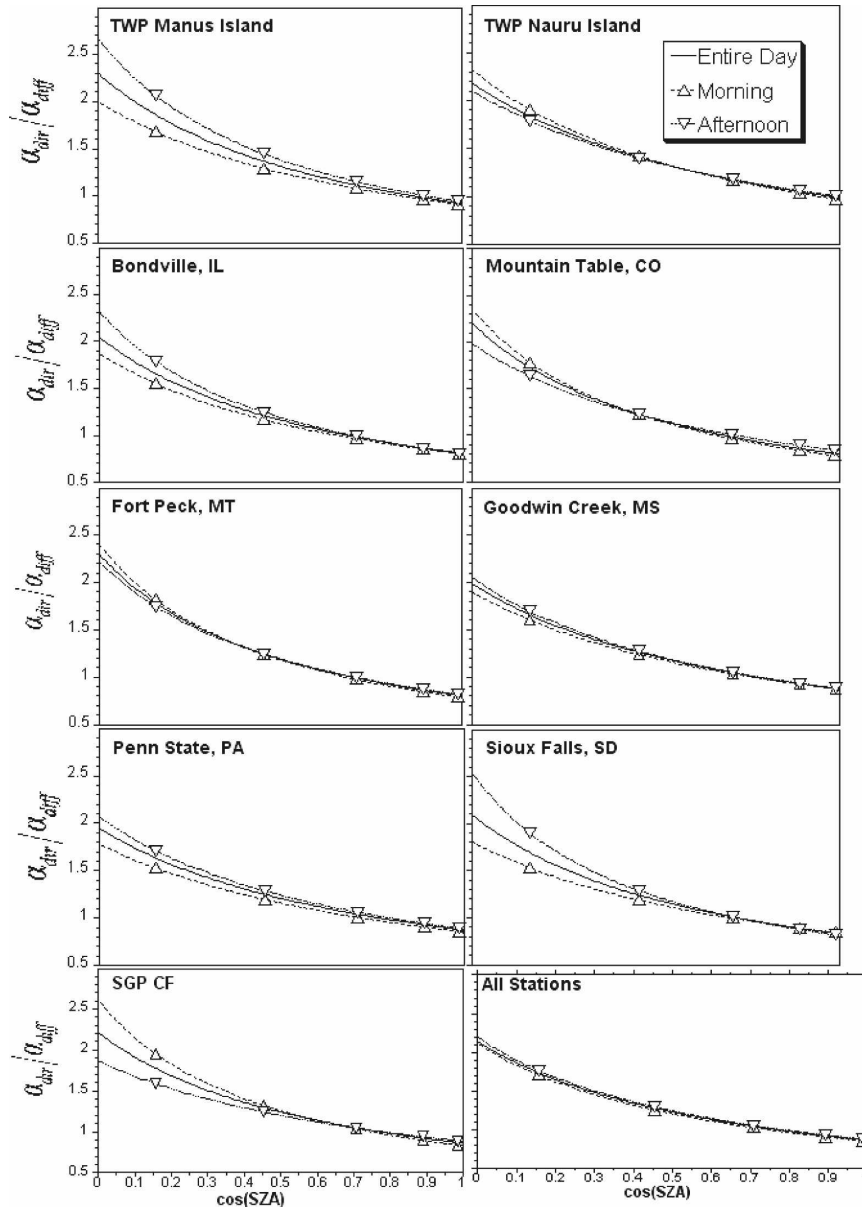


FIG. 10. Dependencies of direct-beam albedo (normalized by diffuse albedo) on $\cos(\text{SZA})$ as determined by the all-sky fits based on observations in the morning, afternoon, or the entire day at each of the nine ARM and SURFRAD stations. The last panel is for the observations at all stations.

type since (2) and (4) use $\alpha_{\text{diff}}^{m,n}$ and $\alpha_{\text{dir}}^{m,n}(60^\circ)$, respectively, as the reference albedo. In the past, it has often been assumed that $\alpha_{\text{diff}}^{m,n}$ is close or equal to $\alpha_{\text{dir}}^{m,n}(60^\circ)$ and the parameterizations (2) and (4) are equivalent.

Analogous to Fig. 7 for the single ARM SGP station, Figs. 10 and 11 show the multistation polynomial fits for $\alpha_{\text{dir}}^{m,n}(\theta)/\alpha_{\text{diff}}^{m,n}$ and $\alpha_{\text{dir}}^{m,n}(\theta)/\alpha_{\text{dir}}^{m,n}(60^\circ)$ that we obtain for each of the nine ARM and SURFRAD stations. At each station three fits based on the morning, afternoon, and entire-day observations are given to depict the di-

urnal asymmetry of the albedo dependence on SZA. The albedos for the TWP Nauru Island and Table Mountain stations show the same diurnal asymmetry as for the SGP CF station. However, the albedos in the morning are not always larger than those in the afternoon at all stations. At the Bondville and Sioux Falls stations the albedos are even larger in the afternoon than in the morning. Minnis et al. (1997) attributed the diurnal asymmetry to the effect of dew on albedo. While dew hardly forms at Table Mountain station, the

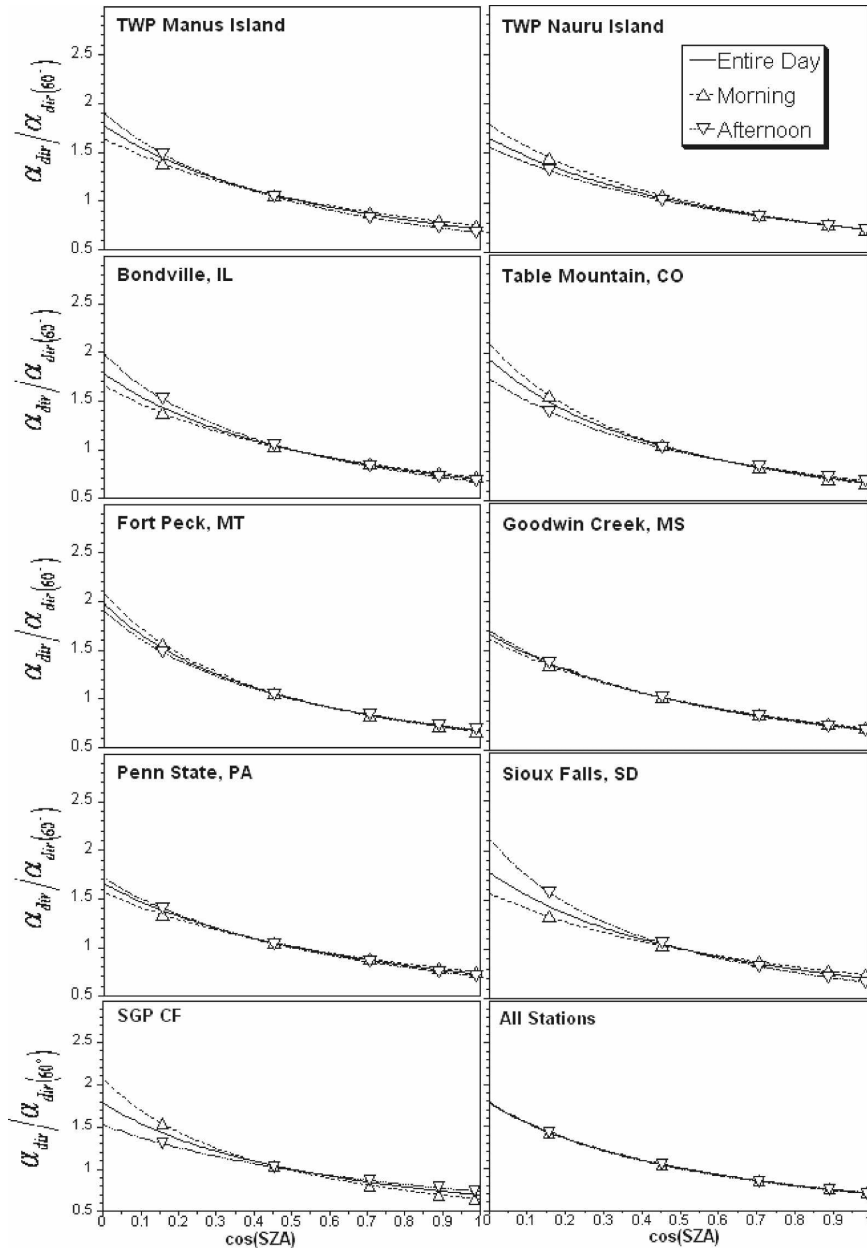


FIG. 11. As in Fig. 10, but the direct-beam albedo is normalized by the direct-beam albedo at $SZA = 60^\circ$.

morning and afternoon contrast of the normalized albedo as a function of SZA is opposite at those two stations. Dew is quite frequent at the Goodwin Creek station, but the normalized albedo shows very little difference between the morning and afternoon. The diurnal asymmetry is not ubiquitous. It is still not clear what causes the morning and afternoon difference of albedos at some stations. At this stage it is impractical to treat the difference in numerical models. In the following we will discuss only the fits based on entire-day observa-

tions. The parameter coefficients for entire-day fits are listed in Table 4.

The entire-day fits for all stations are put together in Fig. 12 for $\alpha_{dir}^{m,n}(\theta)/\alpha_{diff}^{m,n}$ and in Fig. 13 for $\alpha_{dir}^{m,n}(\theta)/\alpha_{dir}^{m,n}(60^\circ)$. The SGP CF site is located at midlatitude and is covered by pastures. The TWP Manus and Nauru stations are in the tropics and are covered by short grasses and bare soil, respectively. The SURFRAD stations (Table 1) are located in the continental United States and are covered by prairie grasses with very few

TABLE 4. Coefficients of the entire-day polynomial fits for each station as shown in Figs. 10 and 11, and for all stations combined as represented by the lines with filled circles in Figs. 12 and 13; $x = \cos(\theta)$.

	$\alpha_{\text{dir}}/\alpha_{\text{diff}} =$		$\alpha_{\text{dir}}/\alpha_{\text{dir}}(60^\circ) =$	
	$(1 + m1)/$	$(1 + m2x)$	$(1 + m1)/$	$(1 + m2x)$
	m1	m2	m1	m2
ARM SGP CF	1.21	1.57	0.779	1.56
ARM TWP Manus	1.29	1.49	0.775	1.49
ARM TWP Nauru	1.18	1.21	0.648	1.26
Bondville, IL	1.05	1.54	0.786	1.58
Table Mountain, CO	1.20	1.76	0.932	1.84
Fort Peck, MT	1.30	1.87	0.978	1.94
Goodwin Creek, MS	0.985	1.27	0.668	1.36
Penn State, PA	0.946	1.23	0.658	1.29
Sioux Falls, SD	1.09	1.52	0.776	1.53
All above stations	1.14	1.48	0.775	1.55

trees at Bondville, Illinois, and Fort Peck, Montana, by rocky desert with scrub vegetation at Table Mountain, Colorado, by pasture grasses with sparsely distributed deciduous trees at Goodwin Creek, Missouri, by grasses and crops at The Pennsylvania State University, Pennsylvania, and by prairie grasses at Sioux Falls, South Dakota (Augustine et al. 2000). In spite of the different surface types, the normalized direct-beam al-

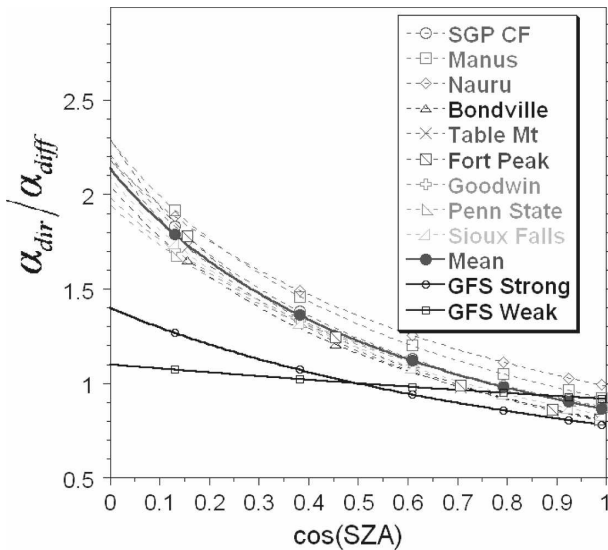


FIG. 12. Dependencies of direct-beam albedo normalized by the diffuse albedo on $\cos(\text{SZA})$. The long-dashed lines represent the empirical fits derived from observations at the ARM and SURFRAD stations as shown in Fig. 10 for the entire-day cases. The thick solid line with filled circles is based on the observations at all stations. The solid lines with open circles and squares are governed by the NCEP GFS parameterization [(7)] with the constant d being set to 0.4 and 0.1, respectively.

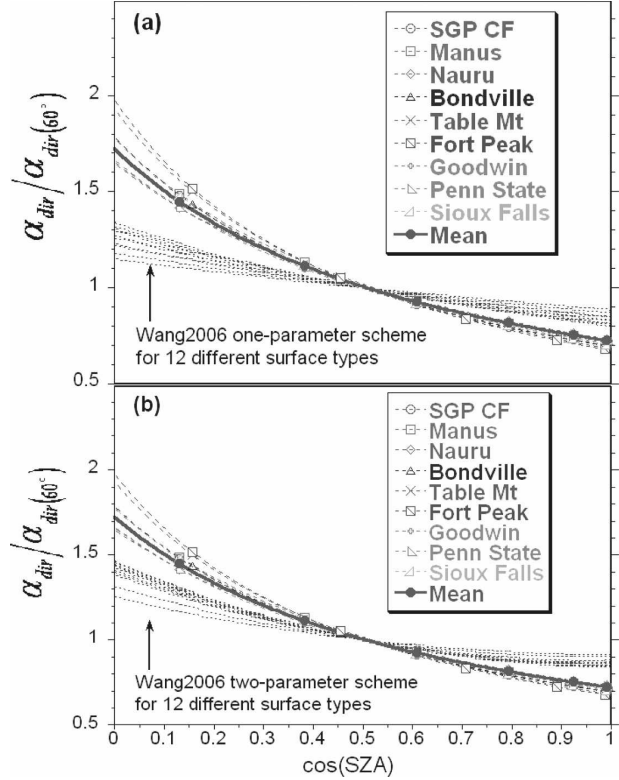


FIG. 13. Dependencies of direct-beam albedo normalized by the direct-beam albedo at $\text{SZA} = 60^\circ$ on $\cos(\text{SZA})$. The long-dashed lines with marks represent the empirical fits derived from observations at the ARM and SURFRAD stations as shown in Fig. 11 for the entire-day cases. The solid thick line with filled circles is based on the observations at all stations. The group of dashed lines without marks are for 12 different land surface types as determined by the Wang et al. (2007) (a) one-parameter and (b) two-parameter schemes based on MODIS products [see Wang et al. (2005) for the desert type and Wang et al. (2007, their Tables 1 and 2) for other surface types].

bedos exhibit quite similar dependencies on SZA at all stations.

We combined the observations at all stations and derived two empirical functions (the lines with filled circles in Figs. 12, 13) that summarize the dependencies of the normalized direct-beam albedos on SZA at the nine ARM and SURFRAD stations. They are applicable for solar fluxes over the entire spectrum or at individual broad bands since we have shown in previous sections that the parameterizations for the normalized direct-beam albedo have almost no dependence on the solar spectrum:

$$f_1(\theta) = \frac{\alpha_{\text{dir}}^{m,n}(\theta, \lambda)}{\alpha_{\text{diff}}^{m,n}(\lambda)} = \frac{1 + 1.14}{1 + 1.48 \cos(\theta)} \quad \text{and} \quad (14)$$

$$f_2(\theta) = \frac{\alpha_{\text{dir}}^{m,n}(\theta, \lambda)}{\alpha_{\text{dir}}^{m,n}(60^\circ, \lambda)} = \frac{1 + 0.775}{1 + 1.55 \cos(\theta)}. \quad (15)$$

These two functions are obtained from limited observations at the ARM and SURFRAD stations, where the surfaces are covered by pasture/prairie grasses, bare soil, rocky desert, or crops. Their applicability for other surface types such as forest and shrub land needs to be tested with additional observations.

As we mentioned earlier, the coefficient d^n from the NCEP GFS parameterization (7) is set to 0.4 (0.1) for surfaces that have strong (weak) dependencies on SZA. These two cases are included in Fig. 12 for comparison with the ARM and SURFRAD fits. The coefficients B_1^n , B_2^n , and c^n in (8) and (9) that Wang et al. (2007) obtained from the MODIS BRDF product were specified differently for 11 different land surface types (see Wang et al. 2007, their Tables 1, 2). The coefficients for the desert case were presented separately in Wang et al. (2005). We used (8) and (9) to compute the normalized direct-beam albedos for the 12 different land surface types. The results are presented in Fig. 13. One can see that the two lines (Fig. 12) governed by the GFS strong and weak parameterizations both show a much weaker dependence of the direct-beam albedo on SZA at all solar zenith angles than does the fit based on the observations. The lines representing the 12 different surface types treated in Wang et al. (2005, 2007) are clustered together, and all are distinctly different from the fits based on the ARM and SURFRAD observations (Fig. 13). The MODIS-based parameterizations give larger direct-beam albedos at local noon and smaller direct-beam albedos at sunrise and sunset than do the ARM and SURFRAD-based fits.

It is noteworthy that in Fig. 13 the fits for the normalized albedos do vary with surface type; however, the difference between the cluster of ARM/SURFRAD fits and the cluster of MODIS-based parameterizations is much larger than the variation within each cluster associated with different surface types. In other words, the uncertainty between the ground and satellite observations is much larger than the albedo difference from different surface types. Within a reasonable degree of accuracy it may not be impractical to use one single function to parameterize the dependence of normalized direct-beam albedo on SZA for all snow-free surface types. It is assumed that the variation of direct-beam albedo with surface type and/or geographical location is represented by the diffuse albedo $\alpha_{\text{diff}}^{m,n}(\lambda)$ from the GFS-type parameterizations and by $\alpha_{\text{dir}}^{m,n}(60^\circ, \lambda)$ from the Wang-type parameterizations, and that the normalized albedo depends only on the solar zenith angle.

7. Summary and discussion

In current climate and weather forecast models a diversity of methods is being used to parameterize land

surface albedos. Their accuracy has been an ongoing subject of discussion. In this study we used the extensive ARM and SURFRAD observations to evaluate the NCEP GFS parameterization (Hou et al. 2002) and those derived from the MODIS products (Liang et al. 2005; Wang et al. 2005, 2007). Results showed that while the diffuse albedo does not change with SZA, the direct-beam albedo strongly depends on SZA. The direct-beam albedo parameterized in the GFS was underestimated at all solar zenith angles, with the largest errors found at sunrise and sunset. The MODIS-based parameterizations underestimated the direct-beam albedo at large solar zenith angles and overestimated it near local noon. The analyses based on all-sky or clear-sky-only samples gave almost identical results, indicating that the influence of atmospheric conditions (e.g., cloud) on the dependencies of surface albedo on SZA is negligible. In contrast to Minnis et al. (1997), this study found that the albedo in the morning is not always larger than that in the afternoon at all stations. A better understanding of the effect of dew on albedo is required before we can treat the albedo diurnal asymmetry in numerical models. It was also found that the uncertainty between the ground- and satellite-based parameterizations is much larger than the variation in albedos in association with different surface types. The MODIS-based parameterizations for 12 different surface types all give much larger (smaller) direct-beam albedos at local noon (sunrise and sunset) than do the ARM- and SURFRAD-based fits.

Based on these results we postulate that even though the direct-beam albedo itself varies with SZA and surface conditions such as soil moisture, canopy, and soil type, the normalized direct-beam albedo may be predominately a function of SZA and has very weak dependencies on other factors. The variations in direct-beam albedo with the season and surface characteristics such as vegetation class and soil moisture (or geographical location) may be adequately represented by the diffuse albedo or the direct-beam albedo at SZA = 60°. These variations were used to normalize the direct-beam albedo in the parameterizations described in this study and can be derived from the MODIS product month by month and band by band with high accuracy and global coverage at a fine resolution up to the pixel level. Therefore, to determine albedos for numerical models one need not refer to or choose a particular land cover classification scheme, which often differs from model to model. At the present stage it is suitable and justifiable from our results to use a single function to parameterize the dependence of the normalized direct-beam albedo on SZA for all land surface types

since the uncertainty in observations is large and their spatial representativeness is limited. The difference between the ground- and satellite-measured surface albedos for the same surface type is much larger than that between the albedos for different surface types from either observation. Ultimately, accurate parameterizations for different surface types need be developed as more and more ground-based and satellite observations that sample over different land surface types with high angular resolution become available. Finally, we emphasize once again that our parameterization is applied to the normalized surface albedo instead of the albedo itself. The latter does vary strongly with land surface type. The normalization is aimed to remove the dependence of the parameterization on land surface type so that it can be applied to all snow-free land points in a model.

Acknowledgments. Fanglin Yang was supported by the U.S. Department of Energy Atmospheric Radiation Measurement Program and the National Centers for Environmental Prediction.

REFERENCES

- Ackerman, T., and G. M. Stokes, 2003: The Atmospheric Radiation Measurement Program. *Phys. Today*, **56**, 38–45.
- Augustine, J. A., J. J. DeLuise, and C. N. Long, 2000: SURFRAD—A national surface radiation budget network for atmospheric research. *Bull. Amer. Meteor. Soc.*, **81**, 2341–2357.
- Barnett, T. P., J. Ritchie, J. Foat, and G. Stokes, 1998: On the space–time scales of the surface solar radiation field. *J. Climate*, **11**, 88–96.
- Bonan, G. B., 1996: A land surface model (LSM version 1.0) for ecological, hydrological, and atmospheric studies: Technical description and user's guide. NCAR Tech. Note NCAR/TN-4171STR, 150 pp.
- Briegleb, B. P., 1992: Delta-Eddington approximation for solar radiation in the NCAR Community Climate Model. *J. Geophys. Res.*, **97**, 7603–7612.
- , P. Minnis, V. Ramanathan, and E. Harrison, 1986: Comparison of regional clear-sky albedos inferred from satellite observations and models comparisons. *J. Climate Appl. Meteor.*, **25**, 214–226.
- Clothiaux, E. E., and Coauthors, 2001: The ARM Millimeter Wave Cloud Radars (MMCRs) and the Active Remote Sensing of Clouds (ARSCL) Value Added Product (VAP). DOE Tech. Memo. ARM VAP-002.1, U.S. Department of Energy, Washington, DC, 56 pp.
- Dai, Y., and Coauthors, 2003: The Common Land Model. *Bull. Amer. Meteor. Soc.*, **84**, 1013–1023.
- , R. E. Dickinson, and Y.-P. Wang, 2004: A two-big-leaf model for canopy temperature, photosynthesis, and stomatal conductance. *J. Climate*, **17**, 2281–2299.
- Dickinson, R. E., 1983: Land surface processes and climate-surface albedos and energy balance. *Advances in Geophysics*, Vol. 25, Academic Press, 305–353.
- Hou, Y.-T., S. Moorthi, and K. A. Campana, 2002: Parameterization of solar radiation transfer in the NCEP models. NCEP Office Note 441, 34 pp.
- Jin, Y., C. B. Schaaf, C. E. Woodstock, F. Gao, X. Li, A. H. Strahler, W. Lucht, and S. Liang, 2003: Consistency of MODIS surface bidirectional reflectance distribution function and albedo retrievals: 2. Validation. *J. Geophys. Res.*, **108**, 4159, doi:10.1029/2002JD002804.
- Koster, R. D., M. J. Suarez, A. Ducharne, M. Stieglitz, and P. Kumar, 2000: A catchment-based approach to modeling land surface processes in a GCM, Part 1, Model structure. *J. Geophys. Res.*, **105**, 24 809–24 822.
- Liang, X.-Z., and Coauthors, 2005: Development of land surface albedo parameterization based on Moderate Resolution Imaging Spectroradiometer (MODIS) data. *J. Geophys. Res.*, **110**, D11107, doi:10.1029/2004JD005579.
- Long, C. N., and T. P. Ackerman, 1997: Detection of clear skies using total and diffuse shortwave irradiance: Calculations of shortwave cloud forcing and clear sky diffuse ratio. *Proc. Sixth Atmospheric Radiation Measurement (ARM) Science Team Meeting*, CONF-9603149, Washington, DC, U.S. Department of Energy, 179–183.
- , —, and J. E. Christy, 2002: Variability across the ARM SGP area by temporal and spatial scale. *Proc. 12th ARM Science Team Meeting*, St. Petersburg, FL, U.S. Department of Energy, 1–16.
- Lucht, W., C. B. Schaaf, and A. H. Strahler, 2000: An algorithm for the retrieval of albedo from space using semiempirical BRDF models. *IEEE Trans. Geosci. Remote Sens.*, **38**, 977–998.
- Lyapustin, A., 1999: Atmospheric and geometrical effects on land surface albedo. *J. Geophys. Res.*, **104**, 4127–4144.
- Matthews, E., 1983: Global vegetation and land use: New high-resolution data bases for climate studies. *J. Climate Appl. Meteor.*, **22**, 474–487.
- , 1984: Vegetation, land-use, and seasonal albedo data sets: Documentation of archived data tape. NASA Tech. Memo. 86107, Washington, DC, 20 pp.
- Minnis, P., S. Mayor, W. L. Smith Jr., and D. F. Young, 1997: Asymmetry in the diurnal variation of surface albedo. *IEEE Trans. Geosci. Remote Sens.*, **35**, 879–891.
- Morcrette, J. J., 2002: The surface downward longwave radiation in the ECMWF forecast system. *J. Climate*, **15**, 1875–1892.
- Oleson, K. W., and Coauthors, 2004: Technical description of the Community Land Model (CLM). NCAR Tech. Note NCAR/TN-461+STR, 174 pp.
- Pinty, B., and Coauthors, 2005: Coupling diffuse sky radiation and surface albedo. *J. Atmos. Sci.*, **62**, 2580–2591.
- Roesch, A., C. Schaaf, and F. Gao, 2004: Use of Moderate-Resolution Imaging Spectroradiometer bidirectional reflectance distribution function products to enhance simulated surface albedos. *J. Geophys. Res.*, **109**, D12105, doi:10.1029/2004JD004552.
- Schaaf, C. B., and Coauthors, 2002: First operational BRDF, albedo and nadir reflectance products from MODIS. *Remote Sens. Environ.*, **83**, 135–148.
- Shi, Y., and C. N. Long, 2002: Best estimate radiation flux value added procedure: Algorithm operational details and explanations. DOE Tech. Memo. ARM-TR-008, U.S. Department of Energy, Washington, DC, 55 pp.

- Stokes, G. M., and S. E. Schwartz, 1994: The Atmospheric Radiation Measurement (ARM) Program: Programmatic background and design of the cloud and radiation test bed. *Bull. Amer. Meteor. Soc.*, **75**, 1201–1221.
- Wang, Z., X. Zeng, M. Barlage, R. E. Dickinson, F. Gao, and C. B. Schaaf, 2004: Using MODIS BRDF/albedo data to evaluate global model land surface albedo. *J. Hydrometeor.*, **5**, 3–14.
- , M. Barlage, X. Zeng, R. E. Dickinson, and C. B. Schaaf, 2005: The solar zenith angle dependence of desert albedo. *Geophys. Res. Lett.*, **32**, L05403, doi:10.1029/2004GL021835.
- , X. Zeng, and M. Barlage, 2007: Moderate Resolution Imaging Spectroradiometer bidirectional reflectance distribution function-based albedo parameterization for weather and climate models. *J. Geophys. Res.*, **112**, D02103, doi:10.1029/2005JD006736.
- Yang, F., H.-L. Pan, S. Krueger, S. Moorthi, and S. Lord, 2006: Evaluation of the NCEP Global Forecast System at the ARM SGP site. *Mon. Wea. Rev.*, **134**, 3668–3690.